LETTER • OPEN ACCESS

Little evidence of hysteresis in regional precipitation, when indexed by global temperature rise and fall in an overshoot climate simulation
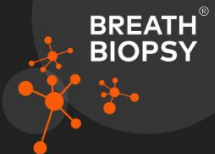
To cite this article: Jeremy Walton and Chris Huntingford 2024 *Environ. Res. Lett.* **19** 084028

View the article online for updates and enhancements.

ENVIRONMENTAL RESEARCH
LETTERS

LETTER

Little evidence of hysteresis in regional precipitation, when indexed by global temperature rise and fall in an overshoot climate simulation

Jeremy Walton[1,*] [ID] and Chris Huntingford[2] [ID]

[1] Met Office Hadley Centre for Climate Science and Services, FitzRoy Road, Exeter, Devon EX1 3PB, United Kingdom
[2] UK Centre for Ecology and Hydrology, Wallingford, Oxfordshire OX10 8BB, United Kingdom
* Author to whom any correspondence should be addressed.

E-mail: jeremy.walton@metoffice.gov.uk

Keywords: precipitation, overshoot, projection, climate hysteresis, Earth System models, two degrees

Supplementary material for this article is available online

Abstract

Society is aiming to stabilise climate at key temperature thresholds, such as global warming at or below 1.5 °C or 2.0 °C above preindustrial levels. However, greenhouse gas emissions are failing to decline, and if they continue on their current trajectory it is likely that such thresholds will be crossed in the decades ahead. Because of this risk, there is an emerging focus on overshoot, where, for a temporary period, global warming is allowed to cross critical thresholds to reach a peak value before decreasing to the desired limit. A key question about overshoots is whether there are hysteresis effects—that is, whether global or regional climate has properties that differ between the phase of global warming increase and the phase of decreasing. Here, we analyse temperature and precipitation data from five Earth System Models (ESMs) forced by the SSP5-3.4-OS CMIP6 overshoot scenario. We look at the level of precipitation during two periods of near-identical global warming: one whilst temperatures are rising, and the other when they are falling. For global means, we find a statistically significant difference between precipitation values during the two periods. This is an example of hysteresis, as the reversion to an earlier global warming state results in a level of global rainfall which is different from that observed when warming was increasing. Spatial disaggregation of rainfall differences between the two near-identical warming levels shows the largest differences in the tropical region, which are statistically significant for four of the five ESMs. When considering much smaller regions, including parts of the tropics, there remains some evidence of hysteresis. However, the differences are no longer statistically significant against a background of substantial interannual rainfall variability. We discuss the implications of our findings for climate impacts assesments.

1. Introduction

Climate change is still a major problem for society, particularly the need for a limit on greenhouse gas (GHG) emissions to prevent dangerous alterations to weather conditions. Upper levels of temperature change that should not be exceeded have been defined—specifically, 2.0 °C (or, in some cases, 1.5 °C [1]) of global warming since preindustrial times. However, achieving these targets requires rapid reductions in future emissions, which poses serious sociological, political and technical challenges [2].

For example, systems providing energy have long lifetimes [3], and even with the most ambitious transitions to non-fossil fuel sources, GHG emissions will likely take decades to reduce massively [4]. Hence, it is likely that prescribed global temperature thresholds will be breached [5, 6]. If society still wants to achieve stabilisation at lower levels, there may be a period of climate *overshoot*, when global mean temperatures are greater than the stabilization target. This raises a concern about whether a return to a lower temperature threshold (potentially by pervasive carbon capture and storage methods) will provide a safe climate.

Specifically, during the overshoot period, the temporary high warming levels may trigger some parts of the climate system to switch to a different state that persists despite falling global temperatures. This is an example of *hysteresis*—the dependence of the state of a system on its history. Our focus here is whether patterns of rainfall are different as global temperatures decline compared to when they are increasing in an overshoot scenario.

Hysteresis is a type of nonlinearity and can be seen to be caused by system inertia which governs the response of components of the system to external forcings, resulting in a delayed system response as forcing increases and decreases. Hence, hysteresis may cause different rainfall features for the same amount of global warming during the heating and cooling overshoot phases. Moreover, hysteresis may be such that large global thermal overshoot causes components of the climate system to cross tipping points [7], which in turn could generate a stronger form of hysteresis where climate features are locked into a new state and stay there, even as global temperatures decline. The climate system is known to contain many feedbacks [8], where rising atmospheric GHG levels may affect parts of the Earth system in a way that slows or accelerates climate change.

The need for a temporary period of global warming above a desired threshold and a better understanding of the effect of hysteresis on the return to a safer climate is focussing attention on the simulation of overshoot scenarios using Earth System Models (ESMs)—see e.g. [9]. ESM components facilitate the investigation of the processes which influence the Earth's climate, and project their interactions with future scenarios of atmospheric GHG levels (see section 2 below for more details). Boucher *et al* [10] used the HadGEM2-ES model to examine hysteresis within an ESM, finding that most Earth system metrics exhibit hysteresis with respect to global temperature levels and atmospheric CO_2 concentration. Using the UVic Earth System Climate Model [11], MacDougall [12] examined the climate response to CO_2 removal and the effect of hysteresis in the global carbon pool. The hysteresis characteristics of the global carbon cycle depend on the rate of removal and climate sensitivity [13].

According to Mitchell *et al* [14], ESM results for the CMIP5 RCP2.6 scenario [15] indicate that the global precipitation rate keeps increasing after surface temperature has been stabilized at order 2.0 °C above pre-industrial levels (see their figure 1(a)). That analysis illustrates that the global Earth system has strong inertial characteristics, with an invigorated global hydrology cycle even for fixed global warming. Specifically, they demonstrate that there is not a unique one-to-one mapping between the level of global warming and global precipitation as climate remains in a transient state even after temperature

is stabilised. By contrast, in their analysis of the results from the CMIP6 ScenarioMIP experiments [16], Tebaldi *et al* [17] find that an overshoot in temperature of a few decades around mid-century, as represented in the overshoot scenario SSP5-3.4-OS, does not influence the final result for temperature and precipitation changes in 2100. These quantities return to the same levels as those reached by SSP4-3.4, although Tebaldi *et al* acknowledge that other aspects of the system may not be as easily reversible.

Mondal *et al* [18] recently made an assessment of the way extreme precipitation is affected by hysteresis, using the CESM1.2 ESM [19] to simulate a scenario where CO_2 is ramped up and then down again. They measure hysteresis by calculating the area under a curve which shows how the climate responds to changing forcing [20]. The curve is different for increasing and decreasing forcing, particularly in monsoon regions.

Here, we study the projections of annual mean temperature and rainfall as determined by five ESMs for SSP5-3.4-OS, a CMIP6 scenario involving a large overshoot in GHG concentrations and global warming. We differ from Mondal *et al* by analysing how rainfall levels change at the global and regional scale for the same levels of global warming—one during the period of rising temperatures, and one when temperature is falling. This does not explicitly consider any hysteresis effects in the relationship between GHG level and global mean temperature, as noted above, but we believe that using the degree of global warming is easier to relate to climate policy, since this often focusses on global warming levels and associated thresholds.

2. Methods

Our scenario of interest, SSP5-3.4-OS [16], prescribes CO_2 emissions associated with SSP5-8.5 up until the year 2040. Beyond 2040, SSP5-3.4-OS incorporates aggressive mitigation which reduces CO_2 emissions from a peak of approximately 70 Gt CO_2 in 2040 to zero in *circa* 2070, and to net negative levels thereafter. These emissions are converted [16, 21] into global mean atmospheric CO_2 concentrations using the MAGICC simple climate model. Hence, land-atmosphere and ocean-atmosphere feedbacks that affect atmospheric CO_2 are as simulated by MAGICC. It is these concentrations (along with the ScenarioMIP-provided concentrations for other long-lived GHGs such as CH_4 and N_2O) which force the ESM simulations whose results we assess here.

ESMs solve partial differential equations which emulate Earth's atmosphere, ocean, cryosphere and land, and include energy exchanges between these components. They predict how these exchanges are expected to change with varying amounts of GHGs. Importantly for climate adaption planning, ESMs

also estimate how near-surface meteorology will change—both globally and regionally—in response to altered levels of radiatively-active gases. The most obvious 'weather' variation is increased temperatures as GHGs rise, which all ESMs project [22], but they also project substantially altered rainfall features in a warmer world [23], and this quantity is the focus of our investigations here.

SSP5-3.4-OS is classified [16] as a Tier 2 experiment—that is, it is not a requirement for modelling centres participating in ScenarioMIP. Hence only a subset of centres have run this scenario using their ESM. Furthermore, we consider only the (relatively small number of) SSP5-3.4-OS simulations which have been extended to 2300. The extension assumes [16, 21] that forcings continue to decline beyond 2100, eventually reaching the (low) levels associated with the extension to SSP1-2.6. It also assumes that the level of negative CO_2 emissions reached in year 2100 remains constant until 2140, when it is increased linearly to reach zero by 2170. Similarly, CO_2 emissions from land use are linearly increased [24] from their negative value at 2100 to zero at 2170, whilst aerosol emissions fall sharply at 2040 to a low value in 2070, decreasing to zero in 2250 [24]. Hence, the balance between aerosol and CO_2 forcings remains qualitatively constant throughout the scenario. Since GHGs are well-mixed whilst aerosols often generate more localised spatial temperature effects, the near-constancy of this ratio suggests that our findings of precipitation hysteresis effects are not caused by a difference in atmospheric gas composition in the warming and cooling phases of the overshoot. Using the extension allows us to more fully capture features in climatological response beyond the standard endpoint of 2100 specfied for many CMIP6 scenarios. This longer timeframe is likely to be important, as climate stabilisation after a mid-century overshoot may not occur until after the end of the century.

We have used the SSP5-3.4-OS extended run's results for UKESM1.0 [9, 25], IPSL-CM6A [26, 27], CESM2-WACCM [28, 29], MRI-ESM2-0 [30, 31] and MIROC-ES2L [32, 33] (see table 1), with a focus on near-surface temperature and precipitation rate (i.e. the CMIP database variables named ***tas*** and ***pr*** respectively). These quantities are presented as ΔT and ΔP, time-evolving anomalies with respect to the IPCC pre-industrial period (1850–1900). We consider the areal-average value of ΔT which acts as our forcing metric for global warming, and analyse ΔP at global and regional scales, examining their time series for evidence of hysteresis.

3. Results

This section describes results from our analysis of ΔT and ΔP from UKESM1.0, before discussing the extent

to which our findings are applicable to the four other ESMs. For brevity, we reserve the diagrams in the main the text for UKESM1.0, presenting corresponding figures for the other models in the supplementary material for this paper. Summary statistics for all models are presented in tables 1–3.

3.1. Global

Figure 1 displays time series for global area-weighted averages of ΔT and ΔP. Both variables increase with time up to *circa* 2070, before decreasing. We note from table 1 that $y_{\Delta T\,\mathrm{max}}$, the year at which ΔT peaks, is earlier than the equivalent year for maximum rainfall, $y_{\Delta P\,\mathrm{max}}$. This observation ($y_{\Delta T\,\mathrm{max}} < y_{\Delta P\,\mathrm{max}}$) is true for all models considered here (table 1), and is the first indication of a potential inertia in rainfall response to changing levels of global warming.

To proceed further, we determine two years at which there is an almost identical level of global warming: one (y_+) during the period of rising ΔT, and one (y_-) when it is falling. Throughout, when comparing mean properties for two years, we use values extracted from a 21 year rolling mean centred on each year, which obviates the effects of variability at interannual scales. After inspecting the behaviour of all models, we choose $y_+ = 2043$, since this falls near the rough midpoint of the temperature range during the period of increasing global warming. For UKESM1.0, the 21 year y_+-centred mean (i.e., for the years between 2033 and 2053) value for ΔT is 2.536 °C (see table 1). During the period of decreasing warming, this temperature is passed in the interval centred on $y_- = 2148$, at which the 21 year centred mean of ΔT is 2.544 °C (for all models, our selected years are such that the relative difference between these two temperature anomalies is less than 1%). The double-headed horizontal arrow in figure 1 highlights the gap between the two years.

In addition to the lag between $y_{\Delta P\,\mathrm{max}}$ and $y_{\Delta T\,\mathrm{max}}$, we see from figure 1 that ΔP has a smaller gradient, so it decreases more slowly than ΔT during its downward phase, again suggesting the potential for inertial effects in precipitation. To quantify whether the difference $\Delta P(y_-)–\Delta P(y_+)$ is statistically significant, we detrend the precipitation values for each year in the two 21 year intervals by first subtracting the 21 year rolling mean centred on that year and then adding the mean value for the midpoint year of the interval. The detrended values are shown in the inset of figure 1 for increasing and decreasing intervals, with the dashed lines denoting the mean at y_- and y_+. We then calculate [34] the t statistic and related p value from a t-test for the means of two independent samples of values. This is a test to see if the null hypothesis that the two samples have identical mean values can be rejected. For UKESM1.0 (see table 1), the large (absolute) value for t (-14.01) and the effectively zero value for p (5.17×10^{-17}) confirm that
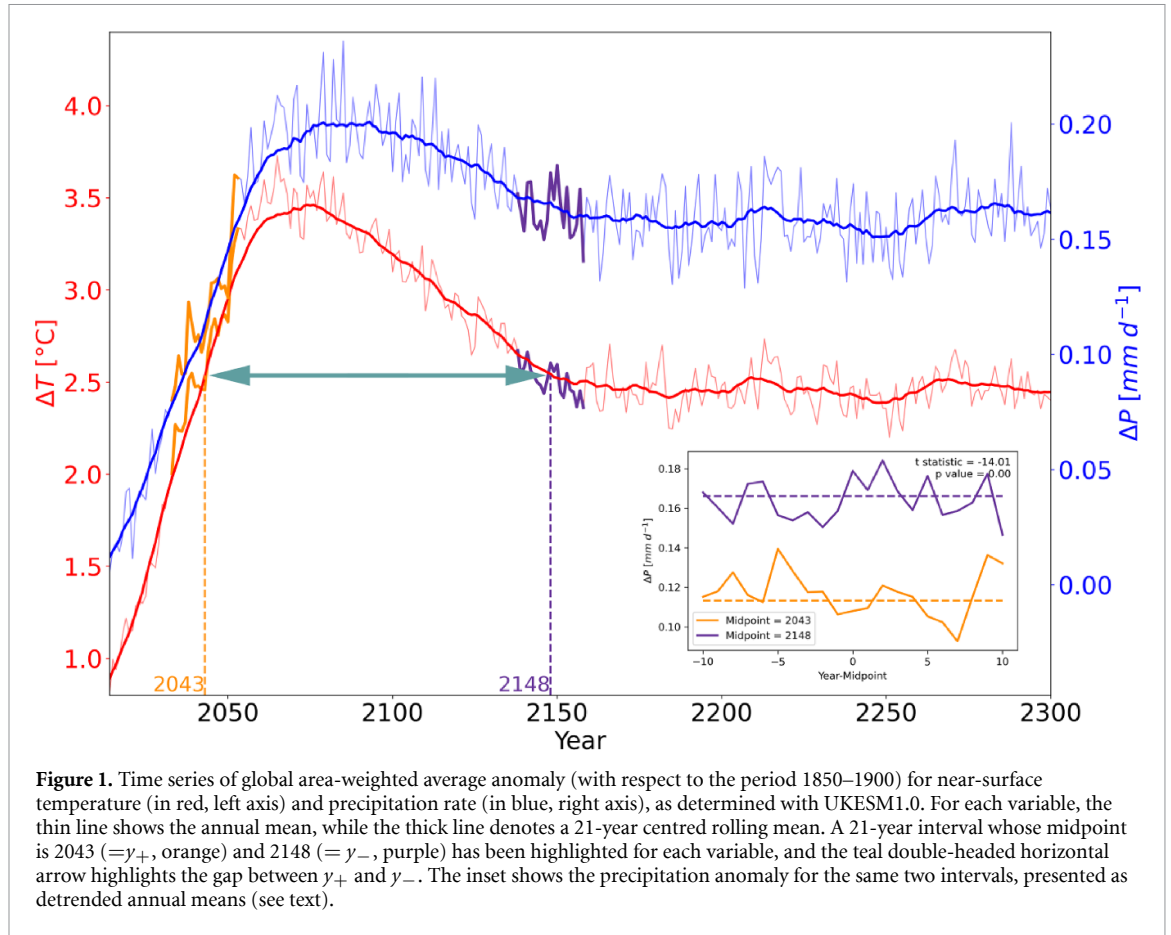
Figure 1. Time series of global area-weighted average anomaly (with respect to the period 1850–1900) for near-surface temperature (in red, left axis) and precipitation rate (in blue, right axis), as determined with UKESM1.0. For each variable, the thin line shows the annual mean, while the thick line denotes a 21-year centred rolling mean. A 21-year interval whose midpoint is 2043 ($=y_+$, orange) and 2148 ($=y_-$, purple) has been highlighted for each variable, and the teal double-headed horizontal arrow highlights the gap between y_+ and y_-. The inset shows the precipitation anomaly for the same two intervals, presented as detrended annual means (see text).
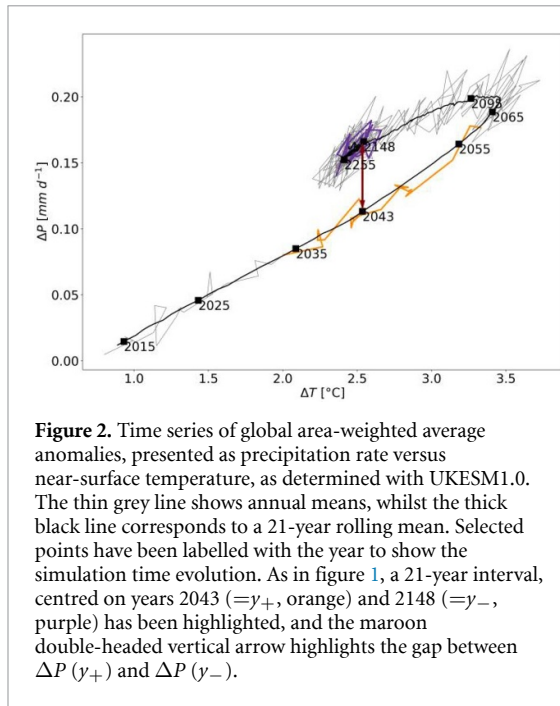
Table 1. Analysis results for the five models. ΔT max is the maximum value of the 21-year rolling mean of the global area-weighted average near-surface temperature anomaly, which occurs in year $y_{\Delta T\,\text{max}}$; similarly for the maximum precipitation rate ΔP max and the year of its occurrence $y_{\Delta P\,\text{max}}$. $\Delta T(y_+)$ is the 21-year centred mean of the global area-weighted average near-surface temperature anomaly at year y_+ during the period of rising ΔT; y_+ has been selected as 2043 in these analyses, while y_- is the year during the period of falling ΔT for which $\Delta T(y_-) = \Delta T(y_+)$ (see text). $\Delta P(y_+)$ and $\Delta P(y_-)$ are the 21-year centred mean of the global area-weighted average of the precipitation rate anomaly at y_+ and y_- respectively. t and p are the results of a t-test on the statistical independence of two 21-year samples of ΔP centred on y_+ and y_- (see text).

Model	UKESM1.0	IPSL-CM6A	CESM2-WACCM	MRI-ESM2-0	MIROC-ES2L
ΔT max [°C]	3.461	3.053	2.956	2.450	2.099
$y_{\Delta T\,\text{max}}$ [year]	2074	2073	2066	2064	2063
ΔP max [mm d^{-1}]	0.201	0.128	0.147	0.113	0.081
$y_{\Delta P\,\text{max}}$ [year]	2093	2087	2088	2072	2086
$\Delta T(y_+)$ [°C]	2.536	2.440	2.410	2.148	1.742
y_+ [year]	2043	2043	2043	2043	2043
$\Delta P(y_+)$ [mm d^{-1}]	0.113	0.087	0.088	0.068	0.037
$\Delta T(y_-)$ [°C]	2.544	2.441	2.412	2.145	1.747
y_- [year]	2148	2130	2112	2089	2107
$\Delta P(y_{2-})$ [mm d^{-1}]	0.166	0.113	0.131	0.107	0.065
t	-14.01	-7.70	-9.67	-10.83	-4.37
p	5.17×10^{-17}	2.00×10^{-09}	5.02×10^{-12}	1.83×10^{-13}	8.70×10^{-05}

the null hypothesis can be rejected. Hence, for global mean changes in precipitation, we conclude that the difference between the average expected values of the two samples is statistically significant. This finding is consistent with the noticeable difference between the two curves in the inset of figure 1. The t and p values for the other models in table 1 also show that

$\Delta P(y_-) - \Delta P(y_+)$ is statistically significant. We therefore conclude that, for these models on a global scale, there is an inertia in precipitation response to global temperature changes in an overshoot setting.

We visualize the same data presented in figure 1 differently in figure 2, which shows ΔP plotted against ΔT, including the 21 year centred rolling

Figure 2. Time series of global area-weighted average anomalies, presented as precipitation rate versus near-surface temperature, as determined with UKESM1.0. The thin grey line shows annual means, whilst the thick black line corresponds to a 21-year rolling mean. Selected points have been labelled with the year to show the simulation time evolution. As in figure 1, a 21-year interval, centred on years 2043 ($=y_+$, orange) and 2148 ($=y_-$, purple) has been highlighted, and the maroon double-headed vertical arrow highlights the gap between $\Delta P\,(y_+)$ and $\Delta P\,(y_-)$.

Figure 3. Global maps of the 21-year mean precipitation anomaly centred on years $y_+ = 2043$ (top panel) and (b) $y_- = 2148$ (middle panel), as determined with UKESM1.0. The bottom panel shows the difference between the two means (centred year 2148 minus 2043). The dark blue and dark red boxes denote respectively the tropical area and the tropical Pacific area (see text) which are used in the regional analysis. The colour bar is common to all panels.

mean and highlight the same 21 year intervals, centred on y_+ and y_- used in figure 1. Here, the fact that ΔP both decreases more slowly than ΔT and that its maximum is delayed, implies that after around year 2070, a clear *hysteresis loop* emerges—that is, for a given ΔT, the value of ΔP post-2070 is greater than the corresponding value on the pre-2070 branch of the curve. The double-headed arrow illustrates the gap between the two branches of the loop at y_+ and y_-, where for almost identical values of global mean ΔT, global mean ΔP differs by $\Delta P(y_-)-\Delta P(y_+) = 0.053$ mm d^{-1} for UKESM1.0 (see table 1). Beyond around 2150, ΔP and ΔT have a smaller dependence on time, (corresponding to the flatter stabilisation period in figure 1), converging to around $\Delta P = 0.15$ mm d^{-1}, $\Delta T = 2.4\,°$C for UKESM1.0.

3.2. Regional

We next study the overshoot projections at the regional scale—in particular, the extent to which our global findings remain applicable at more local scales. Figure 3 shows the spatial distribution of the 21 year centred mean of ΔP—as determined by UKESM1.0—for y_+ and y_- (top and middle panels), and the difference $\Delta P(y_-)-\Delta P(y_+)$ (bottom panel). Points with the largest absolute values for the difference are mostly concentrated around the tropics, here marked as a full latitudinal band of $-20° \leqslant \varphi \leqslant 20°$. The tropical Pacific (for which $102°\text{E} \leqslant \lambda \leqslant 56°\text{W}$) has also been highlighted as a region that contains much of the differences.

Figures 4 and 5 show the time evolution of the area-weighted average anomalies for global near-surface temperature (as seen previously in figures 1 and 2) and precipitation rate in the tropical Pacific region, from UKESM1.0. A comparison with figures 1
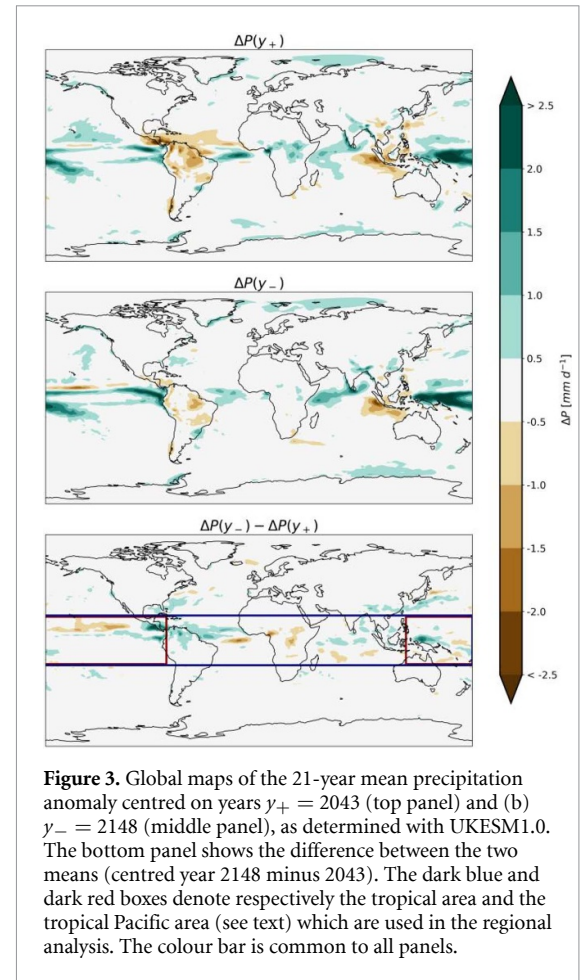
and 2 shows that ΔP still increases with time up to around 2070, but now decreases more slowly. However, the regional data has much more inter-annual variability than the global, due to the smaller number of grid points in the regional sample, likely resulting in a lower amount of spatial cancelling of anomalies compared to the global statistics (see below). For this region, we note from table 2 that $y_{\Delta T \max}$ is earlier than $y_{\Delta P \max}$—i.e. peak temperature is reached before peak precipitation (as was the case on the global scale) for all models apart from MIROC-ES2L (for which $y_{\Delta P \max}$ is only slightly smaller than $y_{\Delta T \max}$).

For this region, the size of the difference $\Delta P(y_-)-\Delta P(y_+)$ as calculated by UKESM1.0 is 0.111 mm d^{-1} (see table 2), which is greater than that for ΔP averaged over the globe—partly because the region we have selected deliberately contains the largest absolute values for this difference. However, despite these larger differences for regional amounts of rainfall for near-identical temperatures the interannual variability is also substantially larger and overwhelms these differences. This large variability makes it harder to discern the gap between the rising and falling ΔT branches in figure 5 and the overlap between the highlighted intervals centred on y_+ and y_-. Once again, we display the overlap (in the inset to figure 4) as
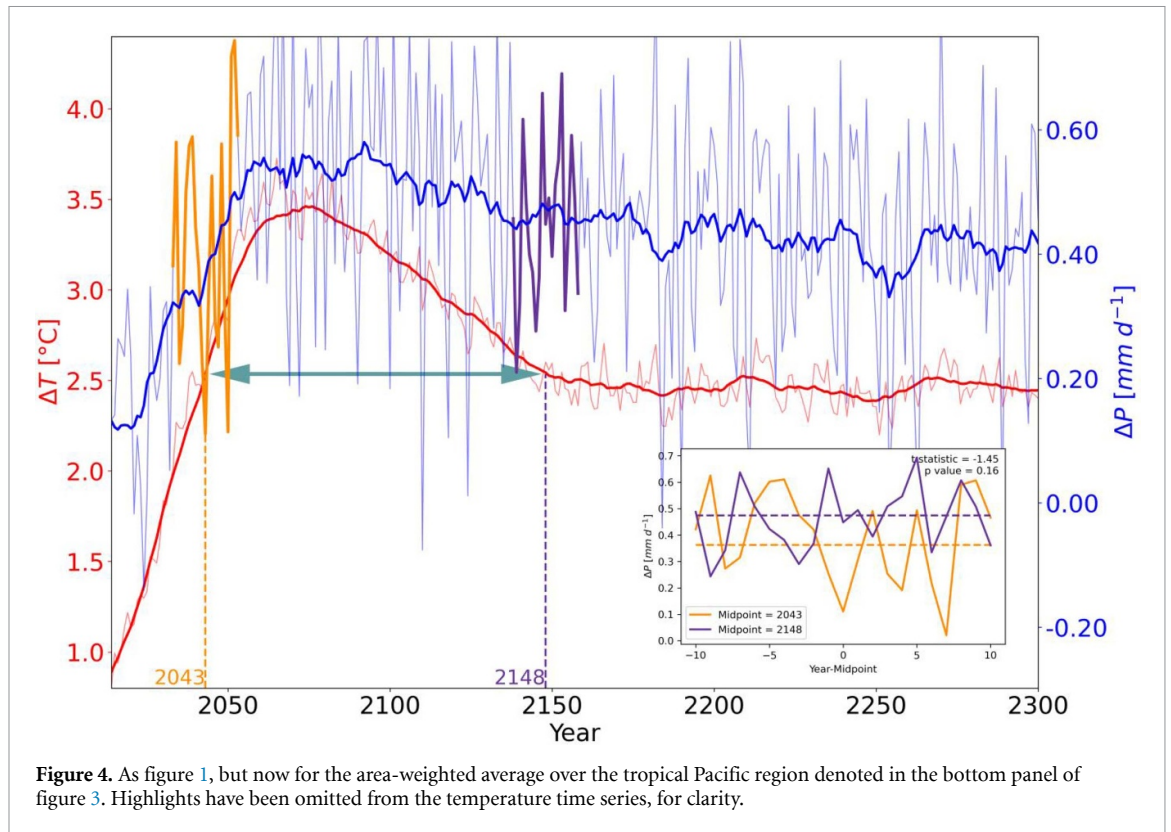
Figure 4. As figure 1, but now for the area-weighted average over the tropical Pacific region denoted in the bottom panel of figure 3. Highlights have been omitted from the temperature time series, for clarity.

Table 2. As table 1, but now for the tropical Pacific region (see text).

Model	UKESM1.0	IPSL-CM6A	CESM2-WACCM	MRI-ESM2-0	MIROC-ES2L
ΔP max [mm d^{-1}]	0.580	0.347	0.511	0.394	0.176
$y_{\Delta P \, \text{max}}$ [year]	2092	2090	2140	2069	2057
$\Delta P(y_+)$ [mm d^{-1}]	0.363	0.219	0.304	0.286	0.074
$\Delta P(y\text{-})$ [mm d^{-1}]	0.474	0.322	0.447	0.351	0.105
t	-1.45	-2.33	-2.11	-1.25	0.02
p	1.56×10^{-01}	2.52×10^{-02}	4.12×10^{-02}	2.17×10^{-01}	9.81×10^{-01}

Table 3. As table 1, but now for the complete tropical region (see text).

Model	UKESM1.0	IPSL-CM6A	CESM2-WACCM	MRI-ESM2-0	MIROC-ES2L
ΔP max [mm d^{-1}]	0.272	0.194	0.230	0.170	0.087
$y_{\Delta P \, \text{max}}$ [year]	2095	2090	2088	2089	2087
$\Delta P(y_+)$ [mm d^{-1}]	0.145	0.132	0.121	0.102	0.038
$\Delta P(y_-)$ [mm d^{-1}]	0.209	0.159	0.197	0.170	0.062
t	-7.30	-2.82	-5.64	-8.61	-1.36
p	7.16×10^{-09}	7.46×10^{-03}	1.51×10^{-06}	1.20×10^{-10}	1.80×10^{-01}

the detrended precipitation values for the two intervals, together with the results of a *t*-test for the means of the two samples. A comparison with the inset to figure 1 shows that the degree of overlap between the intervals is greater for this region, so generating a smaller (absolute) value for *t* (-1.45) and larger value for *p* (0.156). The larger variability prevents rejection of the null hypothesis that there is no statistically significant difference between the average expected values of the two samples. Results from

other ESMs for this region are summarised in table 2, and are consistent with those for UKESM1.0 in that *t* has decreased and *p* has increased compared to global mean $\Delta P(y_-)$ versus $\Delta P(y_+)$. The *p* values range from 0.0252 (IPSL-CM6A) to 0.981 (MIROC-ES2L), indicating moderate to no evidence against the null hypothesis of no difference between $\Delta P(y_-)$ and $\Delta P(y_+)$ for this tropical Pacific location.

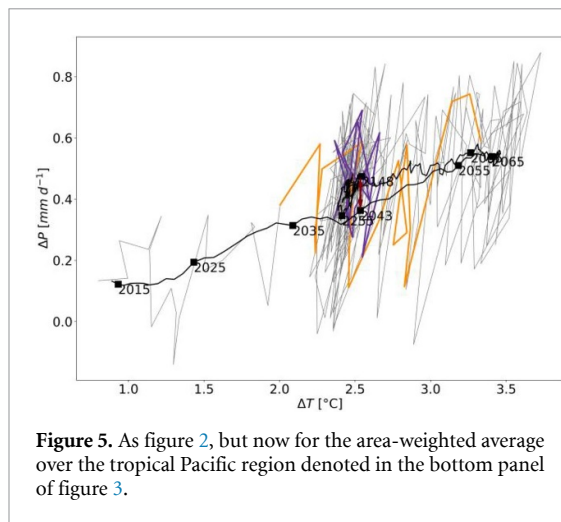For this overshoot scenario, our analysis shows that we have observed hysteresis in the annual mean

Figure 5. As figure 2, but now for the area-weighted average over the tropical Pacific region denoted in the bottom panel of figure 3.

precipitation rate averaged over the globe, but not for the tropical Pacific region. We now consider an intermediate region of all points in latitudinal range $-20° \leqslant \varphi \leqslant 20°$—i.e. the complete tropical zone in figure 3. For brevity, we do not show the equivalent plots, but summarise their characteristics for all models in table 3. We find $y_{\Delta T \max} < y_{\Delta P \max}$ for all models, and also see values for t and p which, for each model, fall between those for the globe (table 1) and the tropical Pacific (table 2). They show that, for this larger region, four models show a statistically significant difference between the average expected values of the samples of ΔP centred on y_- and y_+. The exception is MIROC-ES2L, which has values for t (-1.36) and p (0.18) that are comparable with those for UKESM1.0 in the tropical Pacific—i.e. for this model, there is no statistical significance for $\Delta P(y_-)$–$\Delta P(y_+)$ in the tropical region.

4. Discussion and conclusions

GHG emissions remain sufficiently high that it may be difficult to constrain mean global warming to key targets such as 1.5 °C [5] or 2.0 °C above pre-industrial levels. Hence, if stabilisation of global warming at such targets is still desirable, a period of global temperature overshoot may occur [35]. Alternatively, society may place less initial emphasis on remaining below temperature targets, but global warming could reach levels discovered as dangerous for many populations. Society may then attempt to instigate strong emission cuts, or even initiate negative overall CO_2 emissions, lowering temperatures and following an warming overshoot path. Such overshoots could be large, especially in the latter scenario. Yet it is only recently that the research community has begun to run simulations associated with a substantial peak in temperature.

Understanding the implications of temporary warming peaks is important because the Earth system is believed to include tipping points. Although

some tipping points may have high levels of inertia, allowing a temporary change in temperature that would otherwise cause their activation, others could be triggered at substantially higher levels of global warming [36]. Such non-linearity could cause attributes of the climate system to lock into irreversible states, or have inertial features with timescales comparable to overshoot duration. Both possibilities of hysteresis imply that features of the climate system may be different, for the same global temperature, depending on whether the system is in the warming or cooling phase. Many researchers offer evidence of hysteresis effects—for instance, changes to the land surface that cause land-atmosphere feedbacks to lock climate into a new state, even as warming reverses. Examples include the greening of the Sahara [37], the loss of snow cover [38], or the potential inability of the Amazon rainforest to return to its current state [39]. These behaviours will break correlations between local near-surface meteorological conditions and the background level of global warming. Understanding these differences is critical for adaptation planning, if global mean temperatures follow an overshoot trajectory. However, where they exist, these effects introduce an additional dimension to the projection of climate impacts as they are not simply related to the level of global warming.

We have analyzed features of precipitation from simulations by five ESMs forced by SSP5-3.4-OS. This scenario corresponds to a relatively high peak in global warming before subsequent decline. We have focussed on changes in global mean near-surface temperature and precipitation rate at different geographical scales, and the relationship between them. We use global warming as our metric of climate change as it relates strongly to global policy aspirations (i.e. eventual stabilisation levels). Geographical changes to precipitation affect the future probabilities of drought or flood occurrence and freshwater availability. For all models, we have found evidence of hysteresis [18, 20] in the areally-averaged global mean precipitation. For two periods of near-identical levels of global warming, one when temperatures are rising and one when temperatures fall, we find the latter has higher levels of mean precipitation. Put simply, the world has a potential to be wetter on any return path in global temperature after warming has peaked. Both time periods of comparison are of 21 years and the t-test (95% confidence level) suggests that the means of the two periods are different.

A difference map of the 21 year mean rainfall for the same two periods of near-identical global warming provides details about local contributions to global differences, with the largest discrepancies in the tropics. For the entire tropics, we again find a statistically significant higher rainfall for the decreasing global temperature period (in a similar fashion to the global rainfall) for four out of five ESMs assessed, although the significance level is quantitatively lower.

If we restrict attention to only a longitudinal sector of the Earth's tropical region centred on the Pacific (which contains the largest differences), we cannot reject the null hypothesis (confidence level of 95%) that mean precipitation is different for rising and falling temperatures. We note that our rainfall change results for the tropical region are more germane for adaption planning than those for the tropical Pacific region, which is mostly oceanic.

It is harder to identify hysteresis in local precipitation differences for near-identical global temperature levels because interannual variability is larger at smaller spatial scales. Indeed, when searching for differences in rainfall in individual gridboxes (i.e. over all points in figure 3), for all ESMs, there are no locations where the difference between annual mean precipitation values for rising and falling temperatures is statistically significant. We acknowledge that selecting an averaging interval which is greater than one year would smooth out this variability—for example, using five years would remove effects of the El Niño-Southern Oscillation—and give rise to other potentially stronger conclusions about statistically significant differences. However, we have focussed on interannual variability as it is frequently year-to-year variations which have the strongest societal impacts, and our approach places longer-term hysteresis effects in the context of such yearly fluctuations. The effect of uncertainty caused by interannual variability could also be reduced by performing an ensemble of runs for the SSP5-3.4-OS scenario. A statistically significant difference between average precipitation levels for rising and falling temperatures could be detected with a sufficiently large ensemble. However for many potential overshoot scenarios, the Earth will pass through these periods of similar temperature quickly, and so the high variability can be expected to cause the rainfall levels during the two intervals to be statistically indistinguishable. Hence, regarding annual precipitation, adaptation policy should be predominantly concerned with the background level of global warming, irrespective of whether such warming is rising or decreasing.

We acknowledge three important caveats. Firstly, our analysis is only for a limited set of ESMs, and we hope that our analysis will encourage more model runs within an overshoot-type framework in the planning for CMIP7 [40]. Secondly, our particular scenario peaks and returns relatively quickly—i.e. within decades, rather than over centuries. If a scenario reaches much higher global warming levels and remains there for longer, a more substantial alteration of Earth system components is expected. These changes may involve strong nonlinearities from which

the system may not recover during the period of falling temperatures. Major changes in Earth system features which persist during any declining global warming may modulate any links between large-scale global temperature levels and local climate features during the period of rising warming values. Hence, we encourage modelling groups to simulate overshoot scenarios which incorporate different maximum temperatures and a range of durations at peak warming level. Our third caveat is that the link between climate forcings and global temperature may contain hysteresis effects, even if these are not present in a mapping between global warming and local climate. Specifically, if the linkages between regional meteorological conditions and overshoot in GHG levels or radiative forcing are investigated, stronger hysteresis effects may be observed. There are long timescales, especially oceanic, which break any one-to-one link between radiative forcing (i.e. altered overall composition of radiatively-active gases) and global temperature, and so by definition between radiative forcing and precipitation. For instance, substantial ongoing changes in regional temperature and precipitation patterns have been simulated [41] for stabilised global net-zero CO_2 emissions and related slowly-changing CO_2 levels. Indeed, global precipitation may continue to increase even after a peak in CO_2 concentration has been passed [42]. However, our selection in this paper of global mean temperature rather than radiative forcing 'factors out' many of these longer-timescale effects. We reiterate that this focus on global temperature in our background definition of overall change ties in with the basis for most climate policy being eventual stabilisation at key global mean warming thresholds and the identification of pathways to them [6]. Finally, we acknowledge the effect of other forcing components—including aerosol emissions [43]—on precipitation levels. Their variations are similar to those for CO_2 emissions in this overshoot scenario [24]. However, revisiting our analysis using GHG-only overshoot simulations (as they become available) would formally reveal the extent to which aerosols have any additional regional impacts—beyond hysteresis due to other factors—on the mapping between global temperature and regional precipitation.

We have studied ESM simulations which have been forced by a substantial overshoot scenario, causing an large peak in global warming. At the local level, we find little evidence of statistically different annual mean precipitation levels for similar amounts of global warming in the upward and downward temperature phases. Little or no hysteresis during an overshoot period removes an important

'degree-of-freedom' from climate impacts assessments. This simplification is important when trying to determine the implications of initially missing a global temperature threshold, as it allows a simpler mapping to global temperature without having to refer to other aspects of a global warming path such as its history.

Data availablity statement

Acknowledgments

Conflict of interest

The authors declare that there is no conflict of interest regarding the publication of this article.

ORCID iDs

Jeremy Walton ⓘ https://orcid.org/0000-0001-7372-178X
Chris Huntingford ⓘ https://orcid.org/0000-0002-5941-7770

References

[1] Paris Agreement to the United Nations Framework Convention on Climate Change, Dec. 12, 2015, T.I.A.S. No. 16-1104 2016 (available at: https://unfccc.int/sites/default/files/english_paris_agreement.pdf) (Accessed 12 December 2015)

[2] Intergovernmental Panel on Climate Change (IPCC) 2022 *Global Warming of 1.5 °C: IPCC Special Report on Impacts of Global Warming of 1.5 °C above Pre-Industrial Levels in the Context of Strengthening the Global Response to Climate Change, Sustainable Development, and Efforts to Eradicate Poverty* (Cambridge University Press)

[3] Greiner A, Gruene L and Semmler W 2014 Economic growth and the transition from non-renewable to renewable energy *Environ. Dev. Econ.* **19** 417–39

[4] Fofrich R, Tong D, Calvin K, De Boer H S, Emmerling J, Fricko O, Fujimori S, Luderer G, Rogel J and Davis S J 2020 Early retirement of power plants in climate mitigation scenarios *Environ. Res. Lett.* **15** 094064

[5] Wiltshire A, Bernie D, Gohar L, Lowe J, Mathison C and Smith C 2022 Post COP26: does the 1.5 °C climate target remain alive? *Weather* **77** 412–7

[6] Swaminathan R, Parker R J, Jones C G, Allan R P, Quaife T, Kelley D I, de Mora L and Walton J 2022 The physical climate at global warming thresholds as seen in the U.K. Earth System Model *J. Clim.* **35** 29–48

[7] Lenton T M, Held H, Kriegler E, Hall J W, Lucht W, Rahmstorf S and Schellnhuber H J 2008 Tipping elements in the Earth's climate system *Proc. Natl Acad. Sci.* **105** 1786–93

[8] Ripple W J, Wolf C, Lenton T M, Gregg J W, Natali S M, Duffy P B, Rockström J and Schellnhuber H J 2023 Many risky feedback loops amplify the need for climate action *One Earth* **6** 86–91

[9] Sellar A A *et al* 2019 UKESM1: description and Evaluation of the U.K. Earth System Model *J. Adv. Model. Earth Syst.* **11** 4513–58

[10] Boucher O, Halloran P R, Burke E J, Doutriaux-Boucher M, Jones C D, Lowe J, Ringer M A, Robertson E and Wu P 2012 Reversibility in an Earth System model in response to CO_2 concentration changes *Environ. Res. Lett.* **7** 024013

[11] Weaver A J *et al* 2001 The UVic earth system climate model: model description, climatology, and applications to past, present and future climates *Atmos. Ocean.* **39** 361–428

[12] MacDougall A H 2013 Reversing climate warming by artificial atmospheric carbon-dioxide removal: can a Holocene-like climate be restored? *Geophys. Res. Lett.* **40** 5480–5

[13] Jeltsch-Thömmes A, Stocker T F and Joos F 2020 Hysteresis of the Earth system under positive and negative CO_2 emissions *Environ. Res. Lett.* **15** 124026

[14] Mitchell D, James R, Forster P M, Betts R A, Shiogama H and Allen M 2016 Realizing the impacts of a 1.5 °C warmer world *Nat. Clim. Change* **6** 735–7

[15] van Vuuren D P *et al* 2011 The representative concentration pathways: an overview *Clim. Change* **109** 5–31

[16] O'Neill B C *et al* 2016 The scenario model intercomparison project (ScenarioMIP) for CMIP6 *Geosci. Model. Dev.* **9** 3461–82

[17] Tebaldi C *et al* 2021 Climate model projections from the scenario model intercomparison project (ScenarioMIP) of CMIP6 *Earth Syst. Dyn.* **12** 253–93

[18] Mondal S K, An S I, Min S K, Kim S K, Shin J, Paik S, Im N and Liu C 2023 Hysteresis and irreversibility of global extreme precipitation to anthropogenic CO_2 emission. *Weather Clim. Extremes* **40** 100561ISSN2212–0947

[19] Hurrell J W *et al* 2013 The community Earth System model: a framework for collaborative research *Bull. Am. Meteorol. Soc.* **94** 1339–60

[20] Kim S K, Shin J, An S I, Kim H J, Im N, Xie S P, Kug J S and Yeh S W 2022 Widespread irreversible changes in surface temperature and precipitation in response to CO_2 forcing *Nat. Clim. Change* **12** 834–40

[21] Gidden M J *et al* 2019 Global emissions pathways under different socioeconomic scenarios for use in CMIP6: a dataset of harmonized emissions trajectories through the end of the century *Geosci. Model. Dev.* **12** 1443–75

[22] Lee J Y *et al* 2021 *Future Global Climate: Scenario-Based Projections and Near-Term Information* (Cambridge University Press) pp 553–672

[23] Douville H *et al* 2021 *Water Cycle Changes* (Cambridge University Press) pp 1055–210

[24] Meinshausen M *et al* The shared socio-economic pathway (SSP) greenhouse gas concentrations and their extensions to 2500 2020 *Geosci. Model. Dev.* **13** 3571–605

[25] Good P, Sellar A, Tang Y, Rumbold S, Ellis R, Kelley D and Kuhlbrodt T 2019 MOHC UKESM1-0-LL model output prepared for CMIP6 ScenarioMIP ssp534-over (https://doi.org/10.22033/ESGF/CMIP6.6397)

[26] Boucher O *et al* 2020 Presentation and evaluation of the IPSL-CM6A-LR climate model *J. Adv. Model. Earth Syst.* **12** e2019MS002010

[27] Boucher O *et al* 2019 IPSL IPSL-CM6A-LR model output prepared for CMIP6 ScenarioMIP ssp534-over (https://doi.org/10.22033/ESGF/CMIP6.5269)

[28] Danabasoglu G *et al* 2020 The community earth system model version 2 (CESM2) *J. Adv. Model. Earth Syst.* **12** e2019MS001916

[29] Danabasoglu G 2019 NCAR CESM2-WACCM model output prepared for CMIP6 ScenarioMIP ssp534-over (https://doi.org/10.22033/ESGF/CMIP6.10114)

[30] Yukimoto S *et al* 2019 The meteorological research institute earth system model version 2.0, MRI-ESM2.0: description and basic evaluation of the physical component *J. Meteorol. Soc. Japan* II **97** 931–65

[31] Yukimoto S *et al* 2019 MRI MRI-ESM2.0 model output prepared for CMIP6 ScenarioMIP ssp534-over (https://doi.org/10.22033/ESGF/CMIP6.6927)

[32] Hajima T *et al* 2020 Development of the MIROC-ES2L Earth system model and the evaluation of biogeochemical processes and feedbacks *Geosci. Model. Dev.* **13** 2197–244

[33] Tachiiri K and Kawamiya M 2020 MIROC MIROC-ES2L model output prepared for CMIP6 ScenarioMIP ssp534-over (https://doi.org/10.22033/ESGF/CMIP6.5767)

[34] Seabold S and Perktold J 2010 statsmodels: econometric and statistical modeling with python *9th Python in Science Conf.* (https://doi.org/10.25080/Majora-92bf1922-011)

[35] Huntingford C and Lowe J 2007 "Overshoot" scenarios and climate change *Science* **316** 829

[36] Ritchie P D L, Clarke J J, Cox P M and Huntingford C 2021 Overshooting tipping point thresholds in a changing climate *Nature* **592** 517–23

[37] Hopcroft P O and Valdes P J 2022 Green Sahara tipping points in transient climate model simulations of the Holocene *Environ. Res. Lett.* **17** 085001

[38] de Vrese P and Brovkin V 2021 Timescales of the permafrost carbon cycle and legacy effects of temperature overshoot scenarios *Nat. Commun.* **12** 2688

[39] Boulton C A, Lenton T M and Boers N 2022 Pronounced loss of Amazon rainforest resilience since the early 2000s *Nat. Clim. Change* **12** 271–8

[40] CMIP Phase 7 (CMIP7) - Coupled Model Intercomparison Project (available at: https://wcrp-cmip.org/cmip7/) (Accessed 27 July 2023)

[41] King A D *et al* 2024 Exploring climate stabilisation at different global warming levels in ACCESS-ESM-1.5 *EGUsphere* (https://doi.org/10.5194/egusphere-2023-2961)

[42] Cao L, Bala G and Caldeira K 2011 Why is there a short-term increase in global precipitation in response to diminished CO2 forcing? *Geophys. Res. Lett.* **38** L06703

[43] Persad G 2023 The dependence of aerosols' global and local precipitation impacts on the emitting region *Atmos. Chem. Phys.* **23** 3435–52

[44] Walton J 2024 Data and scripts for figures in Walton & Huntingford, Little Evidence of Hysteresis in Regional Precipitation, When Indexed by Global Temperature Rise and Fall in an Overshoot Climate Simulation *Zenodo* (https://doi.org/10.5281/zenodo.10523162)